



Near-Surface Geophysical Characterization of a Marble Deposit to Promote a Sustainable Small-Scale Mining

Nathália de Souza Penna ¹, Jorge Luís Porsani ^{1,*}, Rodrigo Corrêa Rangel ¹, Victor Hugo Hott Costa ¹,
Nicolas Correa de Oliveira ¹, Marcelo Cesar Stangari ¹ and Conrado de Carvalho Braz de Faria Sousa ²

¹ Departamento de Geofísica, Instituto de Astronomia, Geofísica e Ciências Atmosféricas (IAG), Universidade de São Paulo (USP), São Paulo 05508-010, SP, Brazil; nathaliapenna.usp.br (N.d.S.P.); rodrigocrangel@yahoo.com.br (R.C.R.); victorhugomgb@usp.br (V.H.H.C.); nicolasoliveira@usp.br (N.C.d.O.); marcelo.stangari@iag.usp.br (M.C.S.)

² Mineração Correa Ltda, Campos do Jordão 12460-000, SP, Brazil; gerencia@mineracaocorrea.com.br

* Correspondence: jorge.porsani@iag.usp.br; Tel.: +55-11-3091-4734

Abstract: Small-scale mining (SSM) is responsible for almost all the production of non-metallic minerals in the world and represents around 80% of the mining in Brazil. The lack of direct geological information increases the level of uncertainty associated with the exploratory process, compromises mine planning, limits mineral extraction, and contributes to maximizing environmental issues. In this research, near-surface geophysical methods, including Electrical Resistivity, Capacitive Resistivity, Ground Penetrating Radar (GPR), and Transient Electromagnetic (TEM), were applied to characterize a marble deposit in an SSM located in the Campos do Jordão region, São Paulo state, southeast Brazil. The geophysical methods used provide indirect information about the subsurface geology based on the contrast in electrical and electromagnetic properties. Resistivity results show the efficiency of locating marble deposits, as well as fracture zones. GPR profiles allowed for the investigation of the structural heterogeneities in the subsurface. Geophysical data and lithological information from drill holes were integrated into Micromine software and guided the development of a geological model and a conceptual pit model. The information inferred from the pit modeling allowed us to analyze the potential of the deposit and should be used to assist in developing sustainable mining planning. The results of this work demonstrate that the investment in geophysical research can support the modernization of an SSM and contribute to more sustainable and productive mining.

Keywords: electrical resistivity; capacitive resistivity; tem; GPR; marble; small-scale mining; Brazil



Citation: Penna, N.d.S.; Porsani, J.L.; Rangel, R.C.; Costa, V.H.H.; de Oliveira, N.C.; Stangari, M.C.; Sousa, C.d.C.B.d.F. Near-Surface Geophysical Characterization of a Marble Deposit to Promote a Sustainable Small-Scale Mining. *Remote Sens.* **2024**, *16*, 1147. <https://doi.org/10.3390/rs16071147>

Academic Editor: Amin Beiranvand Pour

Received: 4 October 2023

Revised: 11 December 2023

Accepted: 13 December 2023

Published: 26 March 2024



Copyright: © 2024 by the authors. Licensee MDPI, Basel, Switzerland. This article is an open access article distributed under the terms and conditions of the Creative Commons Attribution (CC BY) license (<https://creativecommons.org/licenses/by/4.0/>).

1. Introduction

Small-scale mining (SSM) is characterized by the exploration of small-scale mineral deposits, which comprises a very diverse and significant portion of the global mining industry. It is estimated that between 15% and 20% of the production of minerals and metals worldwide is associated with SSM [1]. According to the Intergovernmental Forum on Mining, Minerals, Metals, and Sustainable Development (IGF), approximately 80% of the world's sapphire production and about 20% of gold and diamond production come from SSM [2]. In Brazil, SSM is responsible for the entire production of ornamental rocks (e.g., marble, granite, slate, quartzite), gypsum, feldspar, calcite, plastic clays, mica, and tungsten, as well as for more than 90% of the production of sand, refractory clay, and tantalum [3].

SSM is usually characterized by relatively low productivity, application of rudimentary exploration techniques, limited investment, and significant environmental impact due to predatory exploration. A high rate of informality and precariousness of work are also characteristics associated with SSM [1,3,4].

The environmental problems resulting from mining are numerous and include the destruction of natural landscapes and, consequently, degradation of local fauna and flora,

silting up of rivers, irregular disposal of waste and dangerous substances, atmospheric pollution, and pollution of water resources. Mining is essential for economic development; however, it also represents a threat to biodiversity. The development and execution of rational mining planning, which involves an environmental management plan to prevent, monitor, and recover areas affected by exploratory activity, is essential for mining to become sustainable [4–6].

The lack of investment in technical and scientific knowledge to modernize exploration methods constitutes an obstacle to the sustainable development of SSMs. The yield of ornamental rock mining is normally low; it is estimated that only around 20% of the total amount of rock extracted from quarries consists of marketable rock [7–9]. The low productivity observed in most SSM units is related mostly to the application of low-tech, polluting, and inefficient exploration techniques from an operational point of view [3,4,10]. The preliminary geological characterization is an essential step in the development of efficient and responsible mine planning from an economic and environmental perspective. Usually, when technical and scientific criteria are not used to guide mineral exploration, the following cycle is often observed: degradation of the local landscape, including changes in fauna, flora, and water resources; abandonment of the mining; and migration to other areas [5]. The lack of geological knowledge results in increasing environmental degradation limits the productive capacity of SSMs, and increases the level of uncertainty associated with the investment.

The application of non-invasive geophysical methods permits the indirect investigation of the subsurface geological structures of relatively large areas and, thus, can help in the preliminary geological characterization process of mineral deposits, usually saving resources and time when compared to direct investigation methods [11–16]. The integration of geophysical and geological data (i.e., drill holes) allows for the development of a more accurate geological model.

A geological model represents the structures in the subsurface, permits the location of the mineral of interest, and, thus, can be used to guide the mineral extraction process and estimate the extent and even the durability of a deposit. The integration of geophysical and geological data to create a pit model allows for the characterization of the mineral deposit in terms of physical (geometry and extension) and economic aspects [17–19].

In this research, we aimed to demonstrate how the application of near-surface geophysical methods helps in the preliminary geological characterization and, thus, can contribute to a more sustainable and effective exploration of an SSM. In this context, the specific objectives were as follows: (1) apply electrical (Electrical Resistivity and Capacitive Resistivity) and electromagnetic (Ground Penetrating Radar and Transient Electromagnetic) methods to evaluate their potential to characterize a marble deposit; (2) integrate geological and geophysical data to obtain a 3D geological model of the deposit; and (3) develop a conceptual pit model to estimate the dimensions of the marble deposit and evaluate its economic potential.

2. Geology of the Study Area

This research was carried out in the area of the active quarry of Mineração Correa LTD, located in the northeast region of the São Paulo state, in the city of Campos do Jordão (Figure 1).

The study area is located in a Precambrian substrate called Embu Terrane, which consists of a tectonic compartment that is elongated in the NE–SW direction and comprises a Paleoproterozoic basement intruded by granites and metasedimentary cover, including gneisses, schists, quartzites, and marbles [20–22].

In this area, there is a contact between the outcropping marble and the Serra do Alto da Pedra granite, a product of magmatism that occurred between 590 Ma and 560 Ma [22,23]. The Serra do Alto da Pedra Granite is a leucocratic rock that extends in the Embu Terrane as a lenticular body. Apart from the quarry in operation, marble outcrops are not observed in the study area. Data from seven drill holes were made available by the mining company.

The locations of these holes are indicated in Figure 1, and the lithological descriptions are presented in Table 1. As can be seen in Figure 1, the drill holes are concentrated in the northeast direction of the study area. The lithological data from the drillings indicate the occurrence of gneisses and marble.

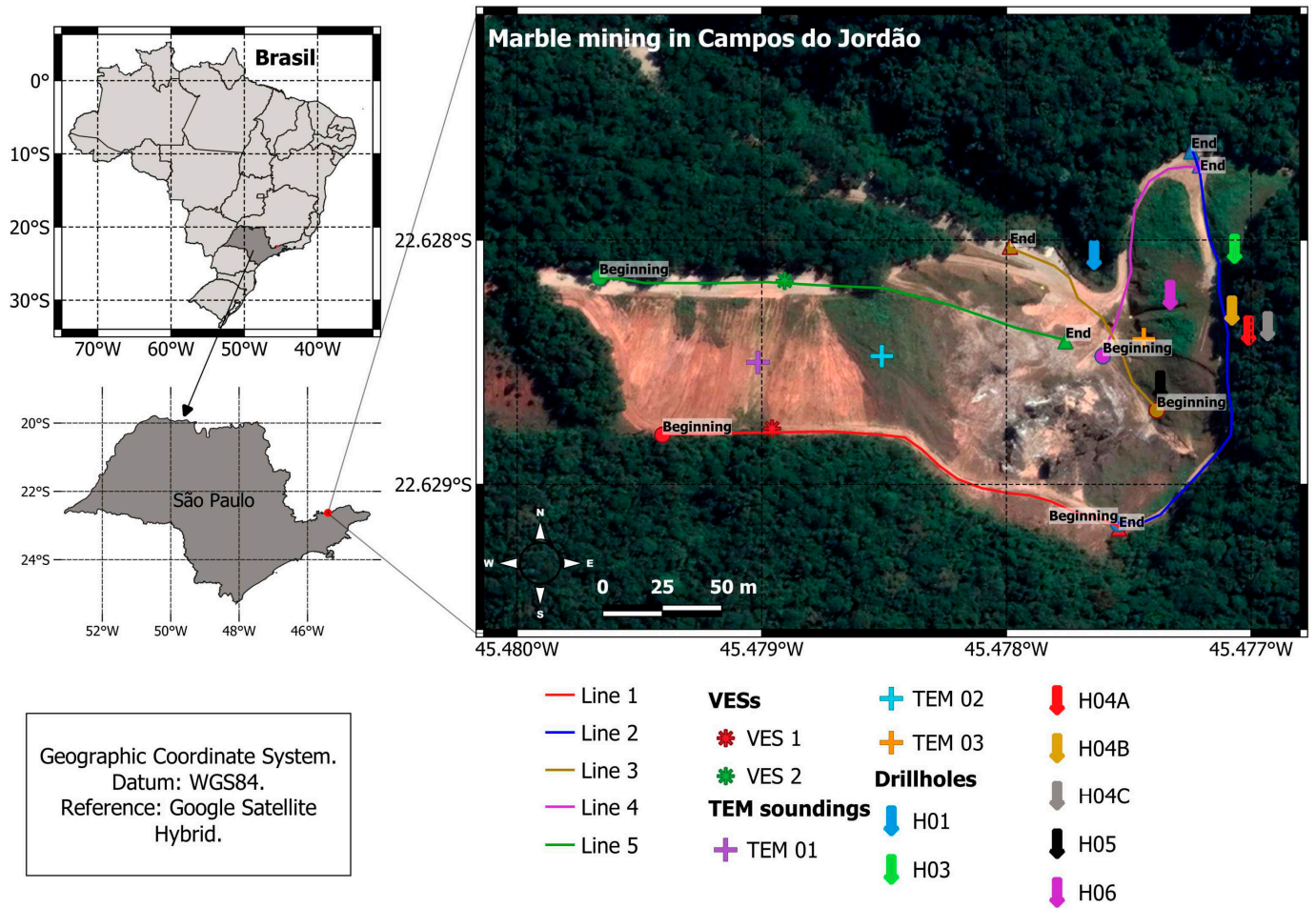


Figure 1. Map of the study area showing the location of the geophysical measurements and drill holes.

Table 1. Lithological information from drill holes (Figure 1).

Drill Holes	Depth (m)	Description
H01	0 to 11.0	Soil
	11.0 to 43.4	Marble
H03	0 to 1.0	Soil
	1.0 to 3.2	Leucocratic gneiss
	3.2 to 26.4	Migmatized gneiss
H04A	26.4 to 80.0	Marble
	0 to 12.0	Soil
	0 to 10.0	Soil
H04B	10.0 to 16.9	Marble
	0 to 3.5	Soil
H04C	3.5 to 12.5	Marble
	0 to 10.0	Soil
H05	0 to 1.9	Soil
	1.9 to 10.1	Marble

3. Materials and Methods

3.1. Geophysical Methods

3.1.1. Electrical Resistivity

Electrical resistivity (ER) is a geophysical method in which artificially generated electrical currents are introduced into the subsurface, and measurements of potential differences are performed on the surface in order to map the distribution of the electrical resistivity [12].

To provide information on the electrical resistivity distribution of subsurface rocks, this method requires at least two pairs of electrodes: a pair of electrodes to inject a direct current or low-frequency alternating current, called current electrodes, and another pair of receiver electrodes in which measurements of potential difference are performed [11,12]. From the electric current (I) and potential difference (ΔV) data, apparent electrical resistivity (ρ_a) values are calculated using the following equation:

$$\rho_a = k \frac{\Delta V}{I} \quad (1)$$

where k is the geometric factor, defined as a function of the arrangement and spacing between the electrodes.

Two techniques for acquiring electrical resistivity data in the subsurface were used in this research: vertical electrical sounding (VES), used to investigate the vertical variation in electrical resistivity in one dimension (1D); and electrical resistivity tomography (ERT), which investigates the vertical and lateral variation (2D) of electrical resistivity in the subsurface [12,24].

3.1.2. Capacitive Resistivity

Capacitive resistivity (CR) is a method of electrical resistivity in which the coupling between sensors and the surface, as the nomenclature suggests, is capacitive. The CR equipment uses coaxial cables with a transmitter and receivers connected to a control unit. The transmitter injects an alternating current (AC) into two coaxial cables (transmitter dipole). The transmitted current is coupled to the surface by capacitance from the coaxial cable. The copper shield (conductor) acts as one plate of the capacitor, the ground surface as the other plate, and the insulating material that makes up the outer skeleton of the cable and separates them, functioning as a dielectric of the capacitor. The receivers are tuned to the transmitter frequency, measure the potential difference in the two cables connected to them (receiving dipole), and send the measured values to the console. Alternating current and the use of an operating frequency avoid interference from electrical cables and telluric currents [25–27].

The use of coaxial cables makes it possible for the CR method to be used on rigid surfaces (such as asphalt or other types of paving, frozen ground, etc.) and highly resistive media, the contexts in which the application of the ER method is limited [28]. Since there is no need to insert the electrodes into the ground, the data acquisition is continuous, which makes it simpler and faster.

3.1.3. Transient Electromagnetic (TEM)

The Transient Electromagnetic (TEM) method is used to investigate the vertical variation (1D) of electrical resistivity in the subsurface from the measurement of the decay of a secondary magnetic field [13,24].

The secondary magnetic field is generated by induction from the variation over time of the primary magnetic field. This method uses a source with direct current, which transmits a pulse, and the measurements are performed when the current is turned off, that is, in the absence of the primary field. In this way, in the TEM method, the signal recorded as a function of time is associated with the electromagnetic response induced in the subsurface. The diffusion time of the induced electrical currents is a function of the electrical resistivity

of the materials [24]. Voltage curves are converted into apparent electrical resistivity (ρ_a) according to the following equation [29]:

$$\rho_a = \frac{k_1 M^{\frac{2}{3}}}{V(t)^{\frac{2}{3}} t^{\frac{5}{3}}} \quad (2)$$

where $k_1 = \mu_0^{5/3} M / 20\pi$, $\mu_0 = 4\pi \times 10^{-7}$ H/m; M is the magnetic moment; $V(t)$ is the normalized voltage measured by a receiver coil, and t is the time.

3.1.4. Ground Penetration Radar (GPR)

Ground Penetrating Radar (GPR) is a geophysical method that uses high-frequency electromagnetic waves, typically between 10 MHz and 2600 MHz, to investigate objects and geological structures in the subsurface. As a result of the frequency range employed, GPR is characterized as a high-resolution electromagnetic method for near-surface geophysical investigations [30,31].

The physical principle of the GPR method is the transmission and reflection of electromagnetic waves. Reflection and diffraction of electromagnetic waves occur at interfaces that separate materials with contrasting electrical properties. At flat interfaces that separate two media with different dielectric permittivity values and/or electrical conductivity, the electromagnetic signal is partially reflected and refracted. The electromagnetic signal reflected toward the surface is recorded as a function of the two-way travel time by a receiving antenna also located on the surface [24,30].

3.2. Acquisition and Processing of Geophysical Data

3.2.1. Electrical Resistivity

VES and ERT data were acquired using Syscal Pro equipment (Iris Instrument, Orléans, France). The ERT data were acquired with a dipole–dipole array in five subareas: lines 1; 2; 3; 4; and 5, which comprise the access roads to the marble quarry (Figure 1).

Table 2 presents the details of the ER, CR, and GPR data acquisition. In lines 1, 2, and 5, the ERT data were acquired with two spacing of current electrodes (AB electrodes), 10 m and 20 m. In lines 3 and 4, the ERT data were acquired with AB electrode spacings of 5 m and 10 m. Two VESs were acquired: one on Line 1 and another on Line 5. The two VESs were performed with the maximum current electrode spacing of 300 m and with a Schlumberger array.

Table 2. Summary of data acquisition parameters for Electrical Resistivity (ER), Capacitive Resistivity (CR), and Ground Penetrating Radar (GPR).

Lines (Length)	Electrical Resistivity	Capacitive Resistivity	GPR
Line 1 (200 m)	Two ERT profiles: AB = 10 m and 20 m. One VES with max. AB/2 = 150 m.	Six profiles: Three with Tx and Rx dipoles distance of 5 m.	One GPR profile with 40 MHz antenna.
Line 2 (200 m)	Two ERT profiles: AB = 10 m and 20 m.	Three with Tx and Rx dipoles distance of 10 m.	One GPR profile with 40 MHz antenna.
Line 3 (100 m)	Two ERT profiles: AB = 5 m and 10 m.	Non-conductive rope of 2.5 m, 5 m, and 10 m lengths	One GPR profile with 40 MHz antenna.
Line 4 (100 m)	Two ERT profiles: AB = 5 m and 10 m.	(variable parameter in the set of 3 profiles).	One GPR profile with 40 MHz antenna.
Line 5 (200 m)	Two ERT profiles: AB = 10 m and 20 m. One VES with max. AB/2 = 150 m.		One GPR profile with 40 MHz antenna.

The ERT data were inverted using the RES2DINV software version 3.4 (Geotomo Software). In order to obtain resistivity models that combined the best lateral resolution and the greatest capacity for in-depth investigation, the data acquired in each line with

different electrode spacings were combined and submitted to a single inversion process. The VESs data were inverted with the IPI2WIN software version 7.01.03 (Geoscan-M LTD, Moscow, Russia).

3.2.2. Capacitive Resistivity

Six CR profiles were acquired on Line 1 (Figure 2) with the OhmMapper equipment (Geometrics Inc., San Jose, CA, USA). Three profiles were acquired with transmitter and receiver dipoles with 5 m length and three profiles with 10 m long dipoles. The length of the rope used in the acquisitions was 2.5 m, 5 m, and 10 m.

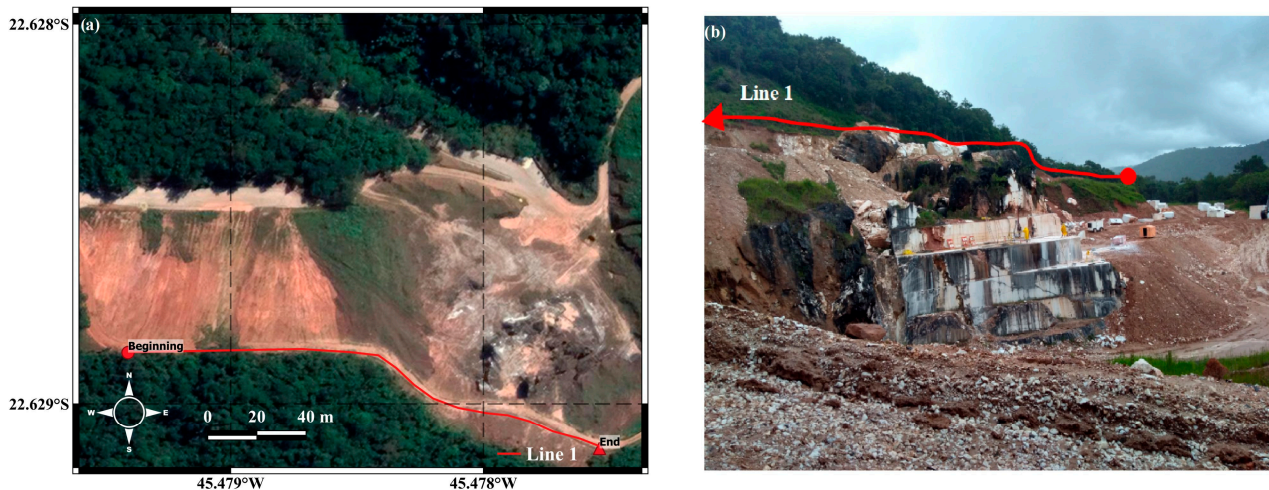


Figure 2. Marble mining: (a) map; and (b) photo showing the location of Line 1 where Electrical Resistivity, Capacitive Resistivity, and GPR data were acquired.

The combined inversion of apparent resistivity data was acquired using 5 m and 10 m dipoles, and 2.5 m, 5.0 m, and 10 m rope spacing was performed in the RES2DINV software, and a 5% change in mean square error (RMS) at each iteration was defined as the limit in the inversion.

3.2.3. TEM

Three TEM soundings were acquired in the study area (Figure 1). The soundings were acquired using a central loop array, and the soundings TEM 01, TEM 02, and TEM 03 had sides with lengths of 70 m, 60 m, and 55 m, respectively. We used a TEM57-MK2 current transmitter, a 3D receiving coil, and the PROTEM-D recorder (Geonics Limited, Mississauga, ON, Canada).

The TEM data were acquired at the three operating frequencies of the transmitter: 30 Hz; 7.5 Hz; and 3 Hz. The inversion of the apparent resistivity data was performed using the IX1D software, version 3.60 (Interpex Ltd., Golden, CO, USA). The inversion results for the 30 Hz frequency presented a better signal/noise ratio. We analyzed the inversion with three different models using smooth, few, and equivalent layers.

The smooth layer model was used to guide the development of a geoelectric model with few layers. The equivalence analysis allows for reducing the ambiguity associated with the few-layers model.

3.2.4. GPR

GPR data were acquired with an unshielded MLF (multi-low frequency) antenna with 40 MHz frequency and a SIR 4000 control unit (Geophysical Survey Systems (GSSI) Inc., Mississauga, ON, Canada).

In lines 1, 2, 3, 4, and 5, GPR profiles were acquired superimposed on the ER profiles (Table 2; Figure 1) in the same direction and length. GPR profiles were processed using

RADAN 7 software (GSSI). The main steps used in data processing were zero-time correction, frequency filters (bandpass 20–70 MHz), temporal background removal filter, spatial stacking filter (Stacking 5 scans), linear gain, and time-to-depth conversion.

To convert from time to depth, we assumed a radar wave velocity of 0.106 m ns^{-1} (relative dielectric permittivity equal to 8). GPR profiles acquired on fractured marble blocks at the mining front were used to estimate the wave velocity [32]. The RADAN 7 software (version 7.6) allows for the propagation speed of the electromagnetic wave to be obtained interactively by adjusting a synthetic hyperbolic curve to the real hyperbola observed in the radargram.

3.3. Geological and Conceptual Pit Models

Mining planning consists of a dynamic mine operation plan developed based on geological, geotechnical, and economic criteria, which should determine the appropriate mining sequencing for rational exploration of the deposit and, thus, optimize the production in the short and long term [19,33,34]. Preliminary geological characterization is an essential step in the development of sustainable mining planning. From the geological characterization of the deposit, it is possible to estimate the relative amount of ore and waste to be extracted, as well as to investigate the economic potential [35–37].

Figure 3 presents a flowchart with the main steps of the workflow used to develop the geological model and the conceptual pit model of the marble deposit. The interpretation of the electrical resistivity models of each sub-area, the lithological data from drill holes, and the topography provided by the mining company were loaded and georeferenced in the Micromine software version 22.5.491.4, where they were used to model the surface topography and build a geologic model for the marble deposit.

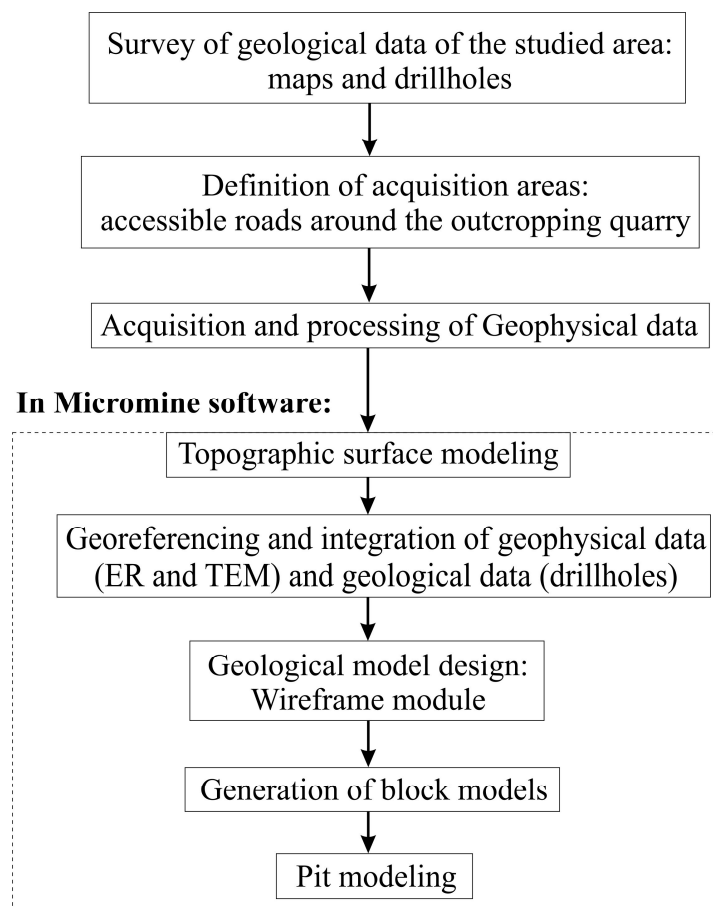


Figure 3. Flowchart with the main steps of the workflow used to develop the geological model and the conceptual pit model of the marble deposit.

In this research, a conceptual pit model was developed in order to exemplify how the geological characterization of the deposit provides quantitative data that allow for a preliminary analysis of the economic potential and the dimension of environmental impact associated with the deposit and, thus, can assist in the development of a rational mining plan: efficient and sustainable from an environmental and economic point of view. To obtain the pit model, we used information provided by the mining company regarding the average density of marble (approximately 2.85 t/m^3), average costs of extracting the overburden, costs of extracting and processing marble, as well as the average sale price of blocks. To determine the limits of the pit, the Micromine software uses the Lerchs–Grossmann algorithm [38].

4. Results and Interpretation

4.1. Geophysical Characterization

4.1.1. Line 1

Line 1 comprises the segment of an access road located around the quarry (Figure 2). Figure 4 presents the geoelectric models with topography correction of the ER (Figure 4a) and CR (Figure 4b) results. The geophysical acquisitions on Line 1 allowed us to correlate the geophysical responses and the marble deposit. It is noted that there is an excellent correspondence between the most surficial structures characterized by a horizon of high resistivity and the occurrence of marbles, as well as a zone of low resistivity related to fractures, probably filled with water.

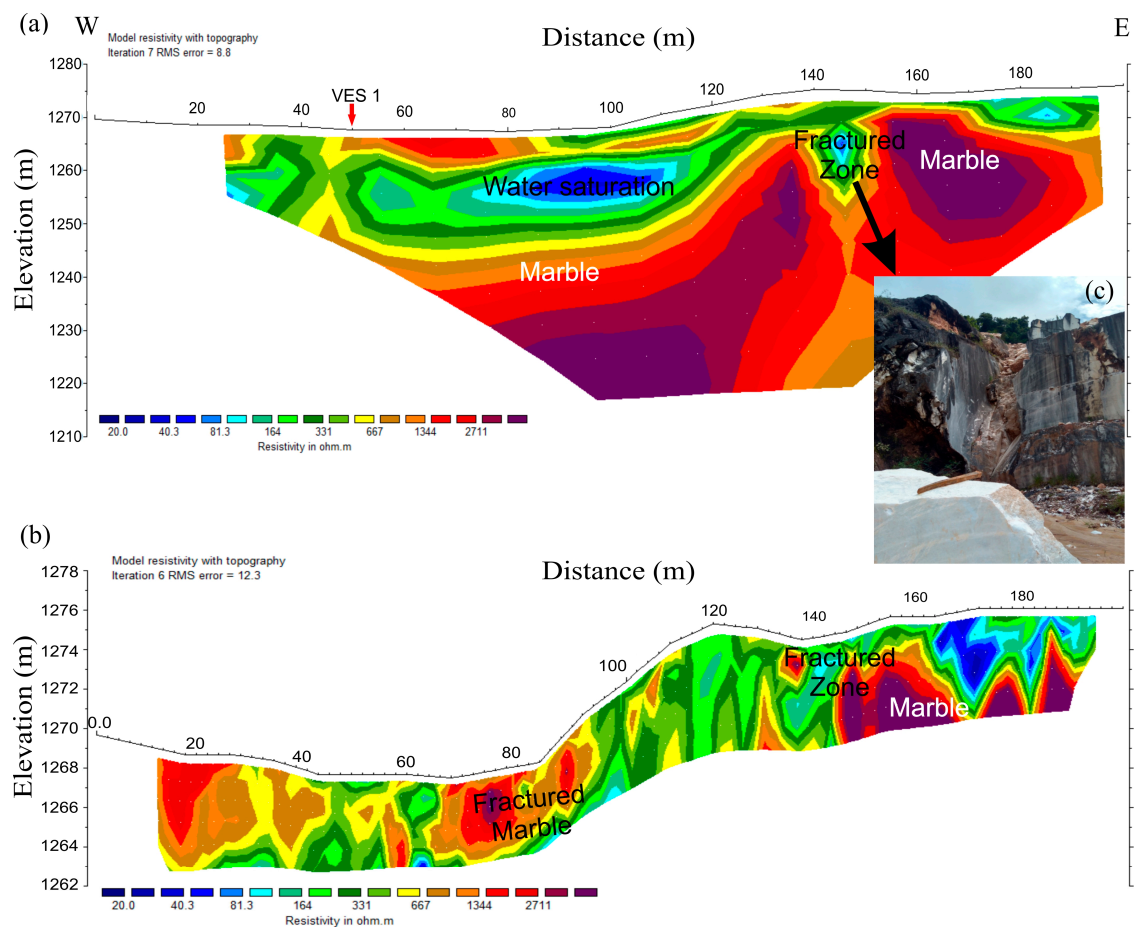


Figure 4. Line 1 geoelectric model: (a) electrical resistivity; (b) capacitive resistivity; and (c) photo of the quarry front showing a subvertical fracture zone.

The ER inversion results of the data acquired with 10 m and 20 m spacing between the current electrodes allowed for investigating the electrical resistivity distribution up to

approximately 55 m in depth (Figure 4a). On the other hand, the CR inversion results of the data acquired with dipole lengths of 5 m and 10 m (and rope lengths of 2.5 m, 5 m, and 10 m) allowed for obtaining a depth of investigation of 6 m (Figure 4b). The limited depth of investigation of the CR method shows that it is recommended to investigate more surficial layers.

The marble deposit is related to higher values of electrical resistivity. The fracture zone observed in the field (Figure 4c) separates two marble blocks partially outcropping on the mining front. According to the geoelectric resistivity model, it is inferred that the outcropping marble blocks extend to approximately 55 m in depth (Figure 4a). It is also observed that the marble body that partially emerges from the west side of the profile presents a lateral continuity and is located below a weathering soil with thickness varying between 5 m and 20 m.

Figure 5 shows the observed data and the geoelectric model of the VES 1 located around the 50 m position on Line 1 (Figure 4). The results complemented the 2D geoelectric model of Line 1 (Figure 4a). Note the presence of two geoelectric horizons with high resistivity in the VES 1 model. The first horizon is characterized by a resistivity of 3500 Ωm and is located below the surficial soil layer. The small thickness of this horizon suggests the occurrence of a crystalline boulder. The second horizon has a resistivity of ~4670 Ωm and has about 17 m thickness, which suggests that it is related to the marble.

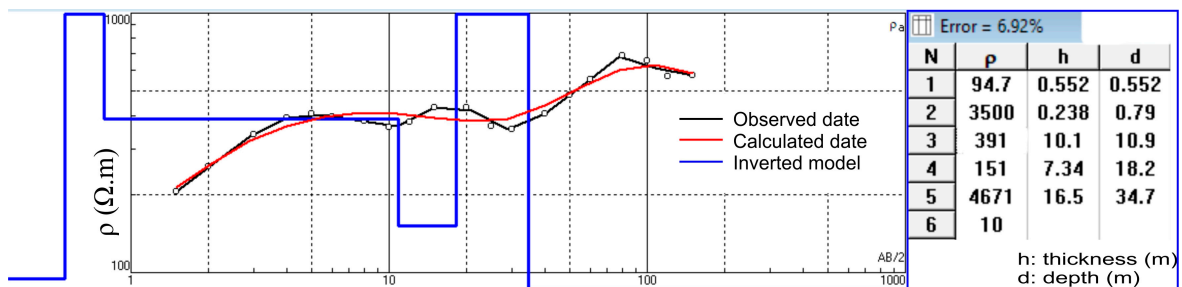


Figure 5. VES 1 electrical resistivity model.

Figure 6 shows the GPR profile of Line 1. The surficial (up to 10 m depth) lateral variation in electrical properties observed in Figure 4 was not observed in the GPR results in Figure 6 because the 40 MHz antenna wavelength does not have the resolution to characterize thin layers.

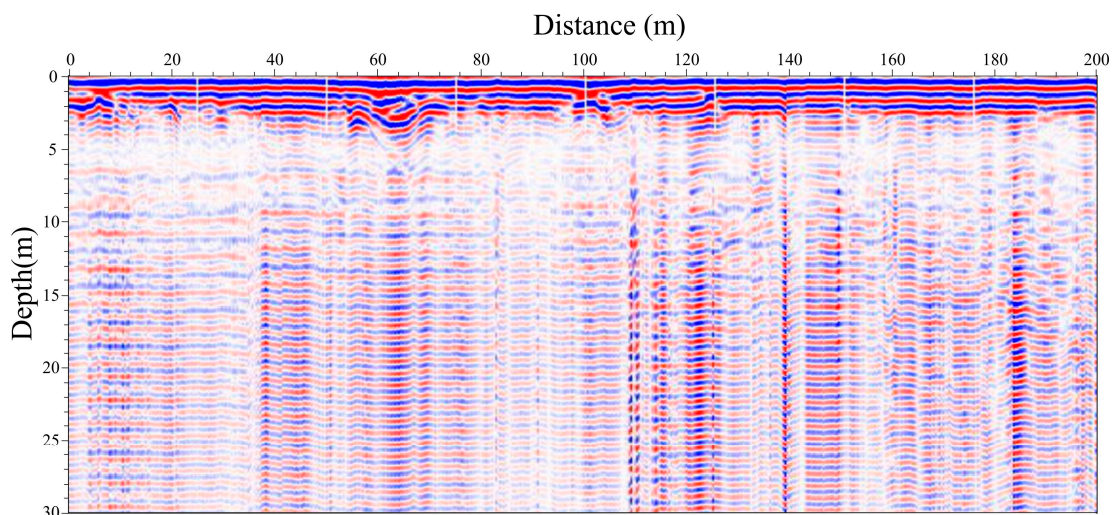


Figure 6. GPR 40 MHz profile of Line 1.

The accentuated irregularity and the presence of many rock fragments in the soil were probably the factors that contributed to the GPR data recorded in this line being extremely

noisy, and, therefore, even after processing, no contrast related to the marble deposit could be observed.

4.1.2. Line 2

Figure 7 shows the geophysical results of Line 2 and the location of drill holes (Figure 1). Similar to the result for Line 1, Figure 7a shows that the most electrical resistive horizons coincide with the depths at which the lithologies of the drill holes indicate the transition from gneiss to marble. A low resistivity observed in the model is probably related to a fracture zone filled with water. The mean squared error of the fit between the observed data and the inverted model was 19.8%, which, despite being considered high, provided an excellent correlation with the lithological data from the drill holes.

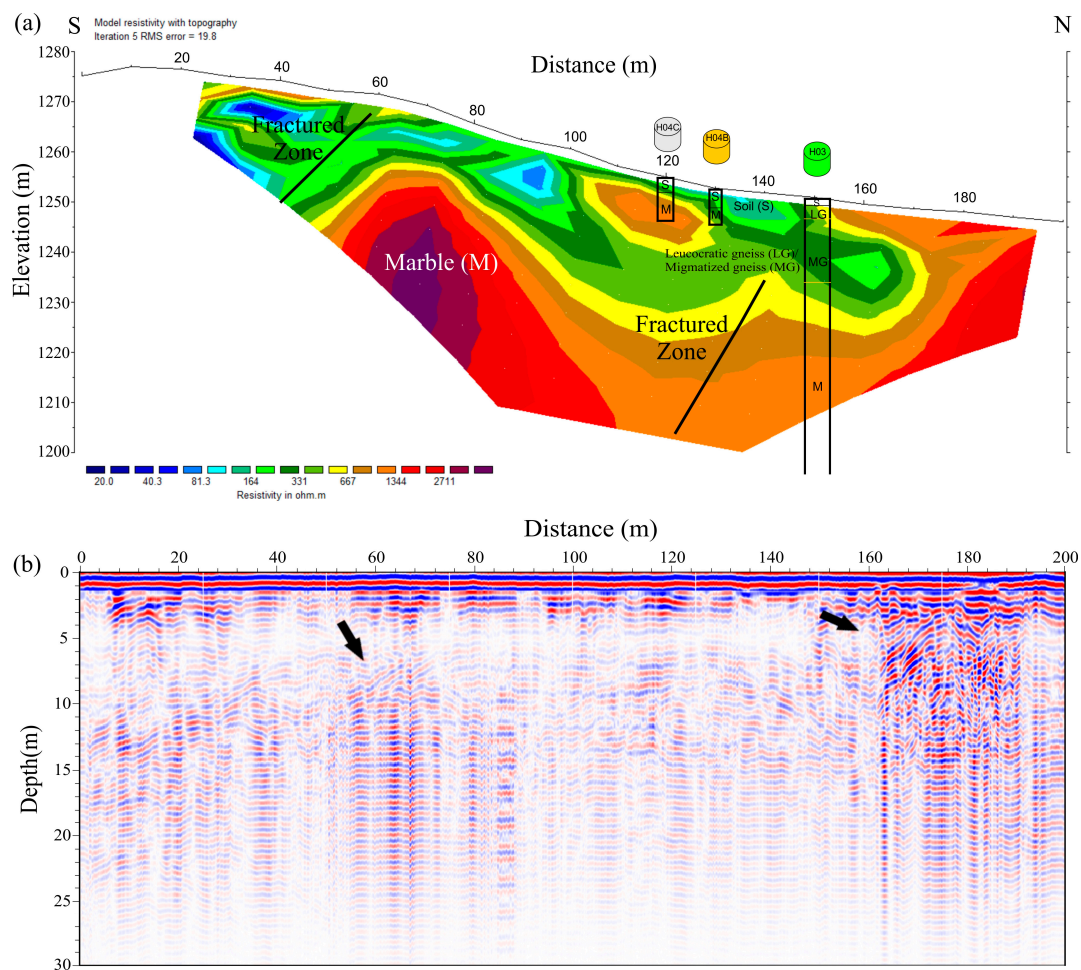


Figure 7. Line 2: (a) Resistivity model; and (b) GPR 40 MHz profile. The lithological information from drill holes H04C, H04B, and H03 are shown superimposed on the Resistivity model (a). The black arrows in (b) indicate overlapping hyperbolic reflections related to fracture zones.

Figure 7b shows the 40 MHz GPR profile. A clear chaotic reflection zone with high amplitude is observed from the 160 m position, which extends to approximately 17 m depth. Comparing the results obtained from the two geophysical methods, it is noted that the zone in which the abrupt vertical and lateral variation in the GPR signal corresponds with the resistivity model to the transition zone from gneiss to marble observed near the surface at the position of approximately 160 m.

The GPR profile is also characterized by a zone with no reflection below approximately 3 m depth that is probably related to the low electrical resistivity soil, as seen in Figure 7a. There is also a reflector between the positions of 40 m and 80 m and from 5 m to 10 m of

depth (black arrow in Figure 7b) that can be related to a fracture zone, as observed in the electrical profile (Figure 7a).

Based on the integration of ER and GPR results, we interpreted that fracture zones are associated with strong resistivity contrasts and hyperbolic reflection patterns in horizontal and vertical directions. Moreover, homogeneous rocks are associated with continuous resistivity and smooth reflections [14–16,39].

4.1.3. Line 3

Figure 8 shows the geophysical results of Line 3 and the location of a drill hole (Figure 1). In Figure 8a, the most electrical resistive horizons show a good correlation with the lithology of the drill hole located close to the 70 m position, coinciding with the presence of the marble. The model shows a geoelectric horizon characterized by low resistivity ($<100 \Omega\text{m}$), which may be related to the presence of fracture zones filled with water on the marble layer. Regarding the marble, the highest resistivity values observed occur from ~ 23 m depth, which suggests the presence of more homogeneous rocks at greater depths.

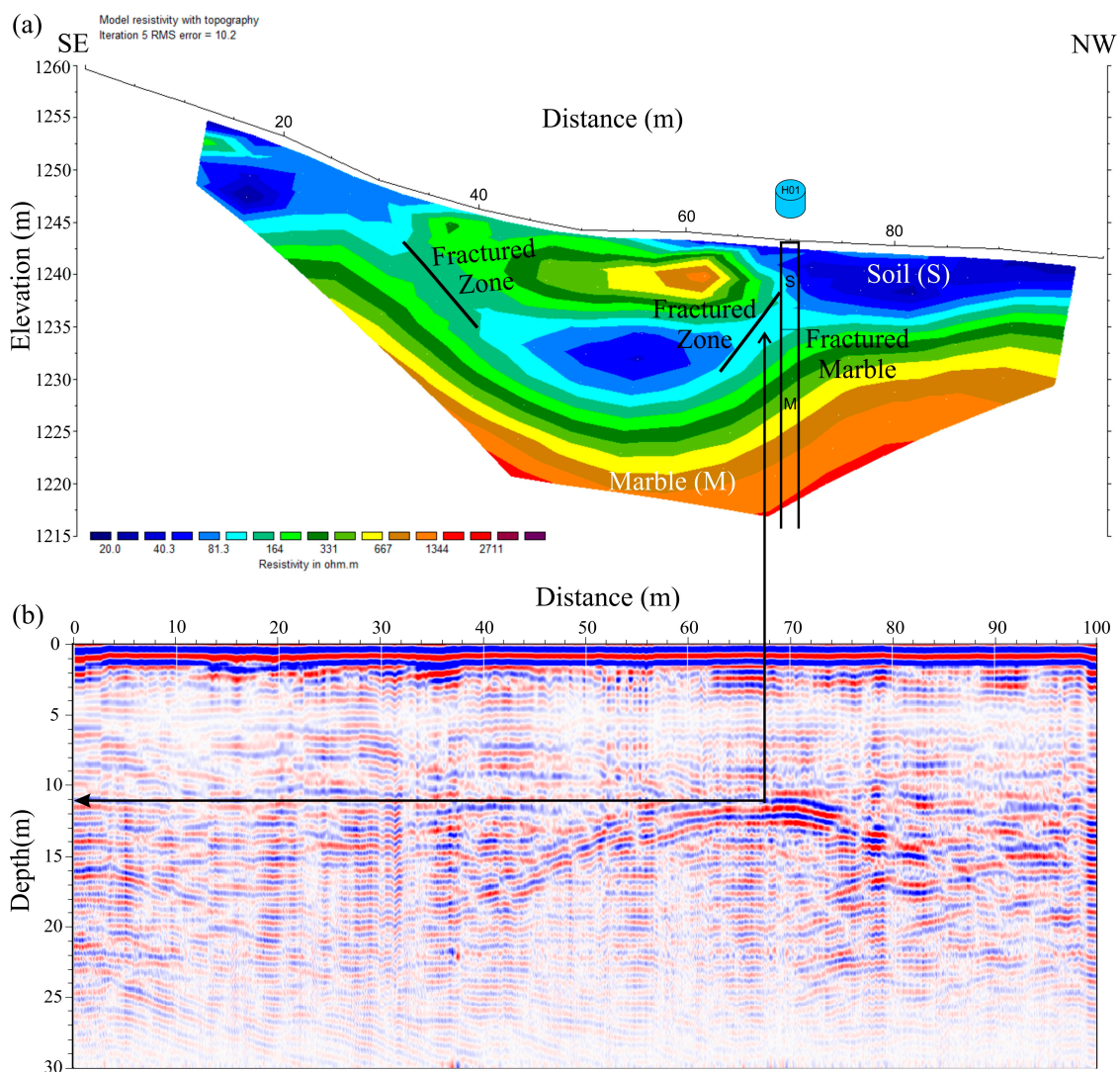


Figure 8. Line 3: (a) Resistivity model; and (b) GPR 40 MHz profile. The black arrow indicates a possible fracture zone.

Figure 8b shows the 40 MHz GPR profile of Line 3. In this profile, a strong reflection is observed between the 40 m and 80 m positions, varying between ~ 11 m and 20 m depths.

The reflection zone shows a good correlation with the low-resistivity zone observed in the resistivity model in Figure 8a. The GPR profile also shows a zone with no reflections up to about 10 m depth along the entire profile. The absence of reflections in the shallow zone may be related to the presence of water-saturated soil and/or more conductive rocks, as suggested in the resistivity model (Figure 8a).

4.1.4. Line 4

Figure 9 shows the geophysical results for Line 4 (Figure 1). In the resistivity model (Figure 9a), a zone of low resistivity is observed up to the 52 m position, followed by an anomalous region characterized by rocks of high electrical resistivity between the 52 m and 100 m positions. The GPR profile (Figure 9b) shows a clear spatial variation constituted by two anomalous regions: one characterized by the absence of reflection up to the 52 m position; and another one by a chaotic reflection pattern between the 52 and 100 m positions that extends to about 15 m depth.

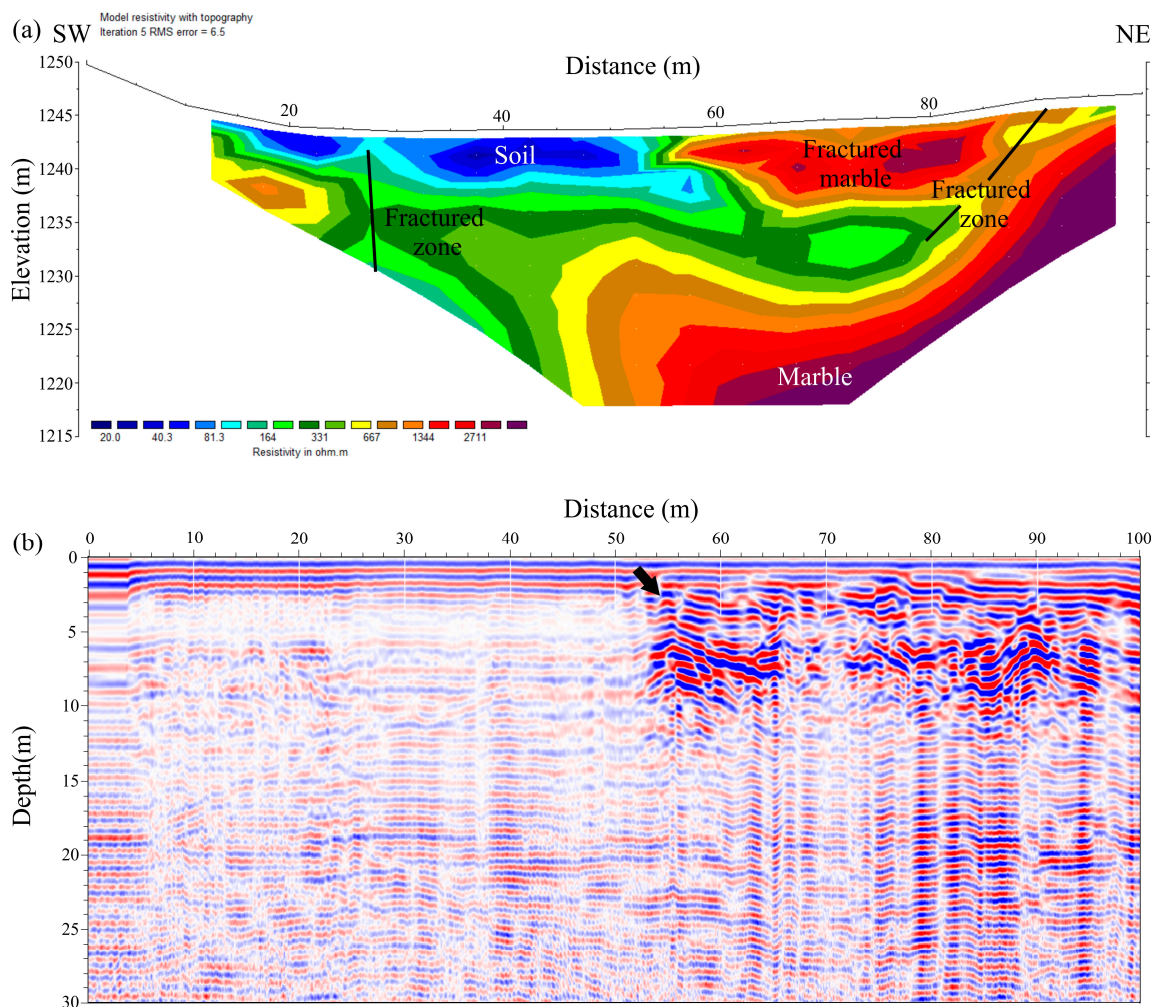


Figure 9. Line 4: (a) Resistivity model; and (b) GPR 40 MHz profile. The black arrow indicates a possible fracture zone.

The region with no radar reflection coincides with the region of low resistivity related to the presence of clayey soil and/or fractures zone with water, which causes attenuation in the GPR signal. On the other hand, the region characterized by chaotic reflections coincides with the region of higher resistivity that may be related to the presence of marble and/or gneiss. To validate the geophysical results, we suggested to drill two holes at positions of 40 m and 65 m.

4.1.5. Line 5

Figure 10 shows the geophysical results of Line 5 (Figure 1). The results suggest a layer of soil with a thickness varying from 3 m to 8 m, followed by a layer of fractured rocks constituted by gneisses and/or marble, varying between the positions of 40 m and 140 m and extending to approximately 50 m depth. From the position of 140 m and a depth of ~35 m, the resistivity model suggests a gradation toward a medium with high resistivity that could be related to the occurrence of marble and/or gneiss. To investigate this hypothesis, more resistivity data and drill holes would be needed.

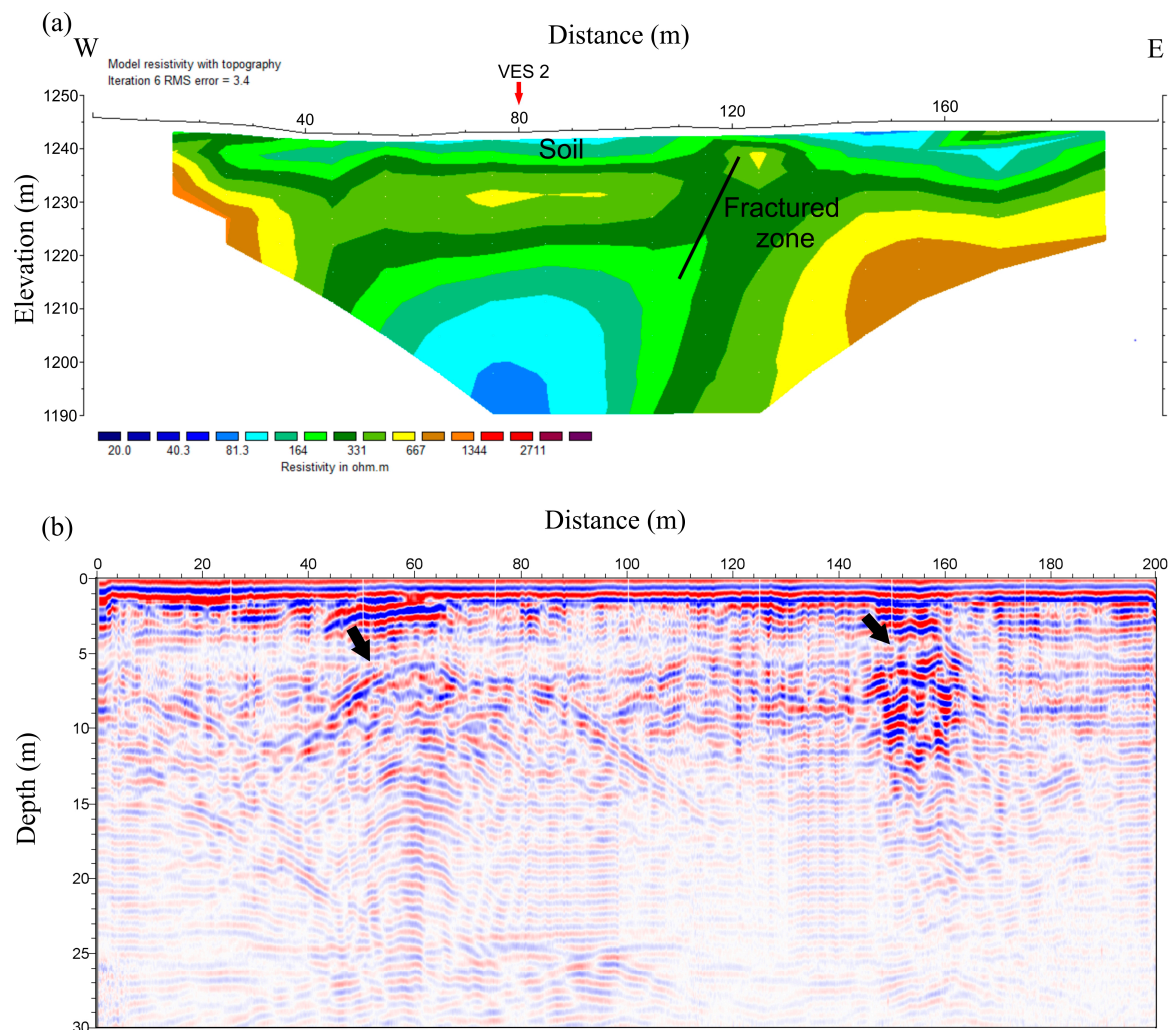


Figure 10. Line 5: (a) Resistivity model; and (b) GPR 40 MHz profile. The black arrows indicate possible fracture zones.

In the GPR profile (Figure 10b), there is a chaotic pattern of reflections from 3 m depth, especially between the 50 m and 170 m positions. Diffraction hyperbolas can be observed up to approximately 25 m depth. Note that the region characterized by chaotic reflections corresponds to a zone with a strong resistivity contrast (Figure 10a), corroborating the interpretation that this region comprises a fracture zone.

Figure 11 shows the VES 2 result located at the 80 m position on Line 5 (Figure 10). There is a geoelectric horizon with high resistivity, around 550 Ωm and 10 m thickness, below a surficial layer of soil and/or fractured rock. The small thickness of this horizon suggests the occurrence of a crystalline rock package limited by fracture zones. The low resistivity of the subsequent geoelectric horizons suggests the presence of a fracture zone filled with water.

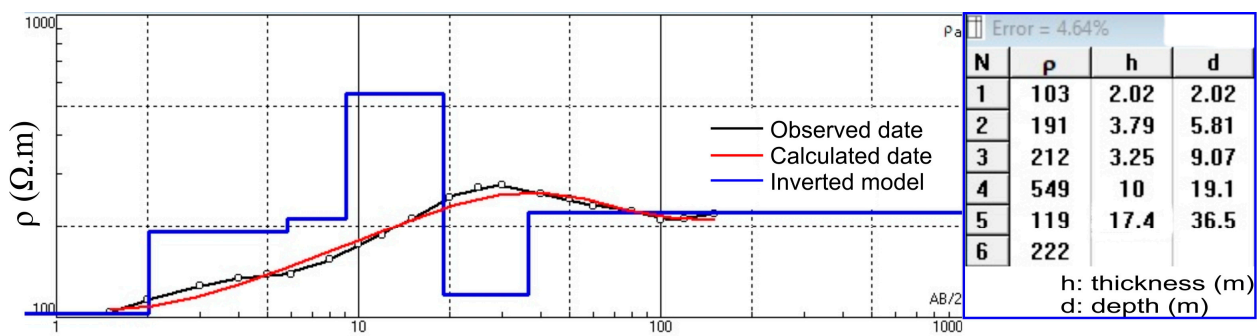


Figure 11. VES 2 resistivity model.

Regarding the correlation between ER and GPR data, it is noted that on Line 2 (Figure 7) and Line 4 (Figure 9), the marble deposits are shallower, and that is why the GPR and ERT results have a good correlation. On the other hand, on Line 3 (Figure 8) and Line 5 (Figure 10), the conductive soil layers are thicker, which tends to attenuate the radar signal; however, the ER and GPR results are still consistent. The only exception is Line 1, where the GPR result (Figure 6) is noisy, and there is a poor correlation with the geoelectrical results (Figure 4).

4.1.6. TEM Soundings

Figure 12 shows the geoelectric models of the TEM soundings 01, 02, and 03 (Figure 1). The geoelectric models of equivalence for the TEM 01 and TEM 02 soundings (Figure 12a,b) comprise two well-defined layers: a horizon with high resistivity that extends to about 350 m and 400 m depth; and a horizon with low resistivity. The horizon characterized by high resistivity, corresponding to the first layer, may be related to a marble and/or gneiss package. On the other hand, the zone of low resistivity associated with the second layer suggests the presence of a fracture zone with water. To verify the occurrence of marble near the TEM 01 and TEM 02 soundings, new drill holes are recommended in this area.

Figure 12c shows the resistivity models associated with the TEM 03 sounding. The equivalence model suggests three well-defined geoelectric horizons. The first is related to a layer with high electrical resistivity, around 500 Ωm with about 110 m thickness. The second horizon is characterized by a layer of low resistivity, varying between 20 Ωm and 30 Ωm , with the base extending to approximately 220 m depth. The top of the third geoelectric horizon is again related to the presence of a more resistive layer at ~200 m depth. Lithological information from drill holes near the TEM 03 sounding and resistivity models for Lines 2, 3, and 4 indicate that the first horizon of high resistivity is probably related to the presence of marble.

4.2. Geological and Conceptual Pit Models

Figure 13 presents the geological model associated with the topographic surface for the marble deposit built from the integration of geophysical results (resistivity profiles, VESs, and TEM soundings) and lithology from drill holes (Table 1). The limits and continuity of marble deposit were defined as follows:

1. The continuity of the marble deposit was inferred from resistivity profiles (Line 2 starts at the end of Line 1; Line 4 crosses Line 2, and Line 3 crosses Line 4) and the drill-hole data (H01, H03, H04B, H04C, and H06);
2. The active quarry (see Figures 2b and 13) was included in the geological model based on the topographic surface;
3. The maximum depth of the resistive layer to the east was defined based on Line 1 ER profiles (~55 m, Figure 4a);
4. The portion of the marble body to the west in the Line 1 resistivity profile had its maximum depth limited by VES1 (~35 m, Figure 5);

5. The top of the marble extending from Line 2 was defined based on the top of the most resistive layer from the resistivity profile (Figure 7a) and borehole data in that area (Figure 1);
6. Finally, the maximum depth of the marble deposit (80 m) that extends from Line 2 was defined based on drill hole H03 (Table 1).

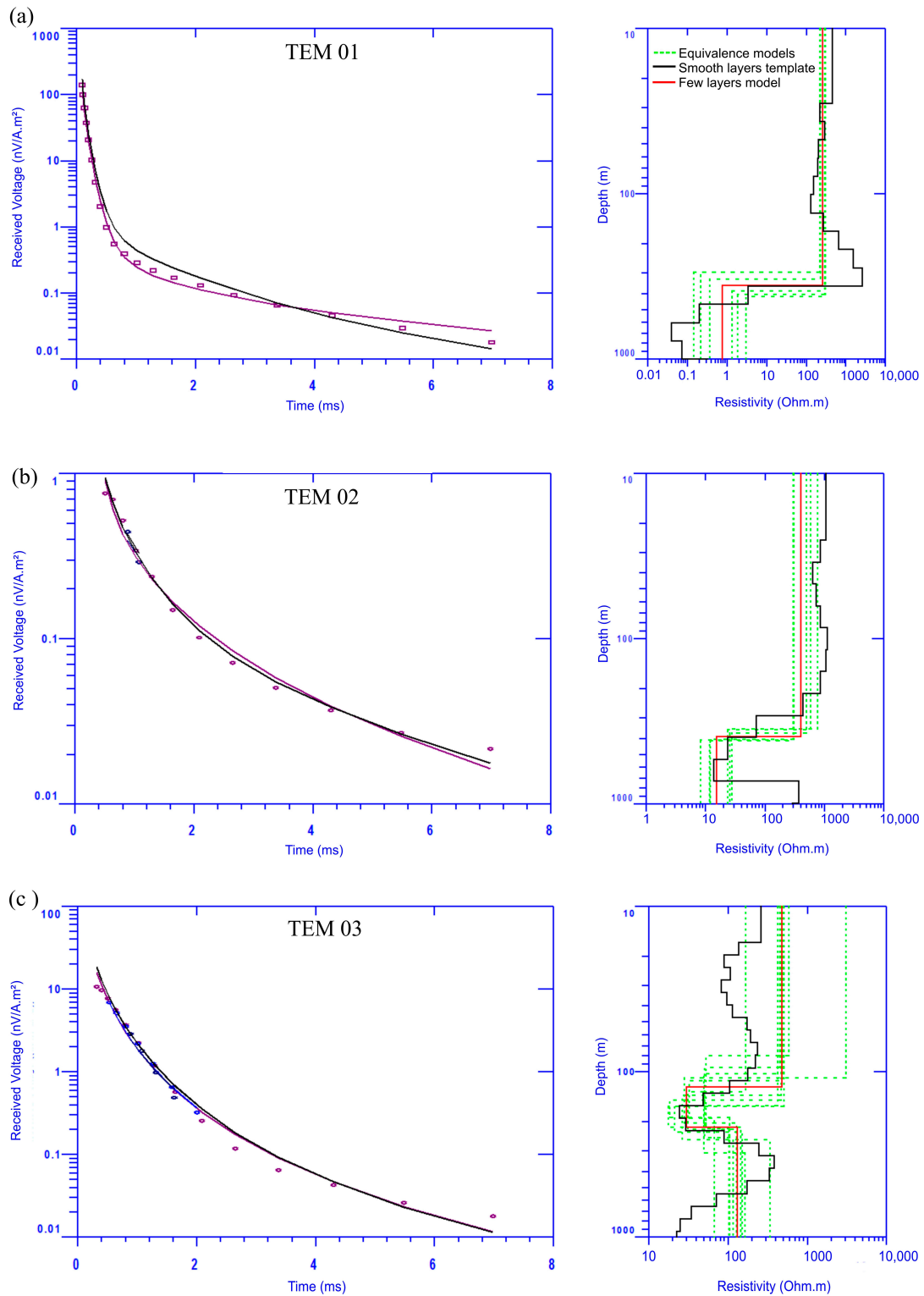


Figure 12. Resistivity model of soundings (a) TEM 01, (b) TEM 02, and (c) TEM 03. On the left side are adjustment curves between observed and calculated data. On the right side are models resulting from the inversion.

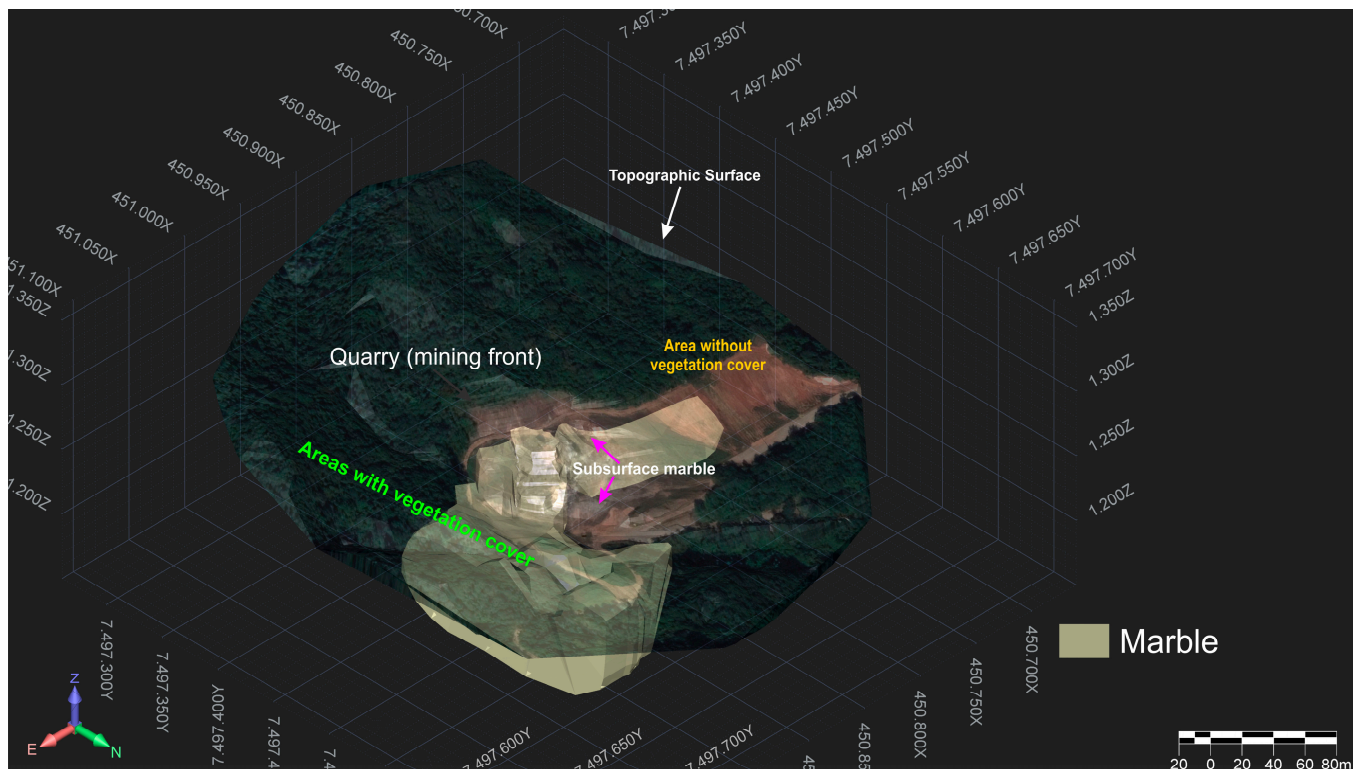


Figure 13. Geological model associated with the topographic surface of the marble deposit.

The information about the marble deposit inferred from the geophysical and geological data was used to develop a pit model. Table 3 presents the mass and volume values, as well as the waste/ore ratio (Strip ratio) and the net present value (NPV) associated with the conceptual pit model of the marble deposit. The net present value was calculated from net revenue and production and beneficiation costs [19,34,36].

Table 3. Marble and waste mass and volume values, strip ratio, and net present value based on the pit model.

Item	Value
Mass of marble (t)	2,344,525
Volume of Marble (m ³)	822,640
Mass of waste (t)	5,374,650
Volume of waste (m ³)	1,990,611
Strip Ratio	2.44
NPV (R\$)	2,250,921,566

Based on the pit modeling, we estimated a possible extraction of 2,344,525 tons of marble and 5,374,650 tons of waste. According to the data in Table 3, the estimated net revenue associated with the exploration of the marble deposit is very promising. Even considering an uncertainty of around 50% in the calculation of the inferred reserve, the marble deposit studied has a very significant economic potential. The estimated data demonstrate that making investments in geological and geophysical research to prove the inferred mineral reserve is strongly recommended.

Near-surface geophysical methods present an excellent cost/benefit, and, as demonstrated in this work, the integration with lithological data allows us to characterize large subsurface areas [13,24]. Additionally, it can be noted that the acquisition of geophysical data allows for optimizing and reducing the costs associated with drill holes. Geological

knowledge not only optimizes mining production but also contributes to minimizing environmental degradation because it can guide the mining to areas where the presence of the mineral of interest is proven [4,5,7,39].

5. Conclusions

The application of geophysical methods enabled the preliminary geological characterization of the marble deposit. The resistivity method allowed for locating the marble and fracture zones up to tens of meters. The GPR profiles located structural discontinuities in the marble in the subsurface. The TEM soundings allowed for investigating a depth of hundreds of meters and contributed to estimating the lateral continuity and the vertical limit of the marble.

Our results demonstrate the effectiveness of using electric and electromagnetic near-surface geophysical methods in the exploration of ornamental rocks. Based on the contrast in electromagnetic properties, these non-invasive methods permit the characterization of structures of interest in the subsurface, including mapping the ornamental rock body and locating structural discontinuities and saturated zones. However, since geophysical methods are indirect, direct geological information is necessary to validate the results.

Geophysical methods combined with lithological information from drill holes allowed for mapping the marble deposit in an SSM. These results demonstrate how the application of geophysical methods in mining can guide exploratory studies to areas where there is a greater probability of occurrence of the mineral of interest and, therefore, can contribute both to optimizing the production and reducing the environmental impact.

The geological model and the conceptual pit model provided relevant information about the deposit, such as the marble mass and volume, which allowed us to evaluate the investment. The net revenue estimated from the inferred reserve indicated that the studied marble deposit had significant economic potential. The initial estimates regarding the amount of waste are relevant for the development of sustainable mining planning, which must include a management and reuse plan for the waste, as well as a recovery plan for the affected areas after the mining is finished.

The results of this work demonstrate that the investment in geophysical research can support the modernization of an SSM and contribute to a more sustainable and productive mining activity.

Author Contributions: N.d.S.P. performed conceptualization, methodology, investigation, formal analysis, resources, data curation, writing—original draft, writing—review and editing, and visualization; J.L.P. performed conceptualization, methodology, investigation, formal analysis, resources, data curation, writing—original draft, writing—review and editing, visualization, supervision, project administration, and funding acquisition; R.C.R., N.C.d.O., V.H.H.C., M.C.S. and C.d.C.B.d.F.S. performed methodology, investigation, resources, data curation, and writing—review and editing. All authors have read and agreed to the published version of the manuscript.

Funding: This research was funded by Fundação de Amparo à Pesquisa do Estado de São Paulo—FAPESP (grant number 2020/15796-9 and 2023/17690-1) and PROEX number (0933/2022).

Data Availability Statement: Data available on request due to restrictions privacy.

Acknowledgments: J.L.P. and N.S.P. thank the Fundação de Amparo à Pesquisa do Estado de São Paulo—FAPESP for providing financial support to develop this research. N.S.P. thanks the Coordenação de Aperfeiçoamento de Pessoal de Nível Superior—CAPES. J.L.P. and N.C.O. thank the Conselho Nacional de Desenvolvimento Científico e Tecnológico—CNPq. We thank the USP/ IAG for providing the infrastructure support. The authors thank Mineração Correa Ltd. for allowing the publication of the results and mining engineer Conrado Braz for logistical and operational support. We thank the students for helping with the data acquisition. Finally, we are thankful for valuable comments and suggestions from reviewers that improve our manuscript.

Conflicts of Interest: The Author Conrado de Carvalho Braz de Faria Sous was employed by the Mineração Correa Ltd. The remaining authors declare that the research was conducted in the absence of any commercial or financial relationships that could be construed as a potential conflict of interest.

The funders had no role in the design of the study; in the collection, analyses, or interpretation of data; in the writing of the manuscript; or in the decision to publish the results.

References

1. Buxton, A. Responding to the Challenge of Artisanal and Small-Scale Mining: How Can Knowledge Networks Help? London: International Institute for Environment and Development. II ED Sustainable Markets. 2013. Available online: <http://pubs.iied.org/16532IIED.html> (accessed on 17 August 2021).
2. Fritz, M.; McQuilken, J.; Collins, N.; Weldegiorgis, F. *Global Trends in Artisanal and Small-Scale Mining (ASM): A Review of Key Numbers and Issues*; International Institute for Sustainable Development (IISD): Winnipeg, MB, Canada, 2018; Available online: <https://www.iisd.org/system/files/publications/igf-asm-global-trends.pdf> (accessed on 20 July 2022).
3. Ministério de Minas e Energia. *Diagnóstico Socioeconômico e Ambiental da Mineração em Pequena Escala (MPE) no Brasil: Relatório Final*; Ministério de Minas e Energia: São Paulo, Brazil, 2018. Available online: <http://antigo.mme.gov.br//documents/20182/d24586f3-bb15-9a72-3b94-693a9ab9b69a> (accessed on 17 August 2021).
4. Seccatore, J. Gestão Sustentável de Recursos e Reservas para Mineração a Pequena Escala. Ph.D. Thesis, Universidade de São Paulo, São Paulo, Brazil, 2014. Available online: https://www.teses.usp.br/teses/disponiveis/3/3134/tde-24042015-145743/publico/TESE_JacopoSeccatore.pdf (accessed on 20 July 2022).
5. Silvestre, C.P.; Da Silva, A.L.C. Problemas ambientais decorrentes da exploração de rochas ornamentais no Município de Santo Antônio de Pádua-RJ. *Rev. Geonorte* **2012**, *3*, 281–289.
6. Macedo, A. O Papel das Cooperativas na Mineração Artesanal e em Pequena Mineração no Brasil. XLV Encontro da ANPAD (EnANPAD), Versão Online 2177–2576. 2021. Available online: https://www.researchgate.net/profile/Alex-Dos-Santos-Macedo/publication/355175573_O_papel_das_cooperativas_na_Mineracao_Artesanal_e_em_Pequena_Mineracao_no_Brasil/links/616469520bf51d4817716875/O-papel-das-cooperativas-na-Mineracao-Artesanal-e-em-Pequena-Mineracao-no-Brasil.pdf (accessed on 20 July 2022).
7. Martínez, J.; Montiel, V.; Rey, J.; Cañadas, F.; Vera, P. Utilization of integrated geophysical techniques to delineate the extraction of mining bench of ornamental rocks (Marble). *Remote Sens.* **2017**, *9*, 1322. [CrossRef]
8. Mello, E.F.; De Almeida, C.N.; Coelho, J.M.; De Barros, L.A.; Araújo, R.N.P. O Polo Produtor de Mármore do Sul do Espírito Santo, Brasil: Ordenamento Territorial e Desenvolvimento Sustentável em Regiões Caracterizadas por Mineração em Pequena Escala. *Anuário Inst. Geociências* **2018**, *41*, 36–51. [CrossRef]
9. Jalalian, M.H.; Bagherpour, R.; Khoshouei, M. Wastes production in dimension stones industry: Resources, factors, and solutions to reduce them. *Environ. Earth Sci.* **2021**, *80*, 560. [CrossRef]
10. Chiodi Filho, C.; de Paula Rodrigues, E.; Artur, A.C. Panorama técnico-econômico do setor de rochas ornamentais no Brasil. *Geosciences* **2004**, *23*, 5–20.
11. Telford, W.M.; Geldart, L.P.; Sheriff, R.E. *Applied Geophysics*; Cambridge University Press: Cambridge, UK, 1990.
12. Kearey, P.; Brooks, M.; Hill, I. *Geofísica de Exploração*; Oficina de textos: São Paulo, Brasil, 2009.
13. Dentith, M.; Mudge, S.T. *Geophysics for the Mineral Exploration Geoscientist*; Cambridge University Press: Cambridge, UK, 2014.
14. Luodes, H. Natural stone assessment with ground penetrating radar. *Est. J. Earth Sci.* **2008**, *57*, 3. [CrossRef]
15. Uhlemann, S.; Chambers, J.; Falck, W.E.; Tirado Alonso, A.; Fernández González, J.L.; Espín de Gea, A. Applying Electrical Resistivity Tomography in Ornamental Stone Mining: Challenges and Solutions. *Minerals* **2018**, *8*, 491. [CrossRef]
16. Magnusson, M.K.; Fernlund, J.M.; Dahlin, T. Geoelectrical imaging in the interpretation of geological conditions affecting quarry operations. *Bull. Eng. Geol. Environ.* **2010**, *69*, 465–486. [CrossRef]
17. Periotto, A.J. Determinação da Cava Ótima em Mineração a Céu Aberto Através de Programação Paralela. Ph.D. Thesis, Universidade Federal do Rio de Janeiro, Rio de Janeiro, Brazil, 1992. Available online: <https://www.pesc.coppe.ufrj.br/uploadfile/1339608654.pdf> (accessed on 22 July 2022).
18. Caccetta, L.; Hill, S.P. An application of branch and cut to open pit mine scheduling. *J. Glob. Optim.* **2003**, *27*, 349–365. [CrossRef]
19. Flores, B.A.; Cabral, I.E. Análise de sensibilidade na otimização econômica de uma cava. *Ver. Esc. Minas* **2008**, *61*, 449–454. [CrossRef]
20. Fernandes, A.J.; Campos Neto, M.C.; Figueiredo, M.C.H. O Complexo Embú no leste do Estado de São Paulo: Limites e evolução geológica. Master's Thesis, Universidade de São Paulo, São Paulo, Brazil, 1991. Available online: https://www.teses.usp.br/teses/disponiveis/44/44134/tde-29082013-160727/publico/Fernandes_mestrado.pdf (accessed on 14 December 2023).
21. Janasi, V.A.; Alves, A.; Vlach, S.R.F.; Leite, R.J. Granitos peraluminosos da porção central da Faixa Ribeira, Estado de São Paulo: Sucessivos eventos de reciclagem da crosta continental no Neoproterozóico. *Geol. USP* **2003**, *3*, 13–24. [CrossRef]
22. Trouw, R.A.J.; Peternel, R.P.M.; Duffles, P.; Vinagre, R.; Coutinho, G.R.; Matos, G.C.D.; Ramos, R. Geologia e Recursos Minerais da Folha Pindamonhangaba SF. 23-YB-VII, Estados de Minas Gerais e São Paulo. 2020. Available online: <https://rigeo.cprm.gov.br/xmlui/handle/doc/17707> (accessed on 27 July 2022).

23. Heilbron, M.; Valeriano, C.M.; Tassinari, C.C.G.; Almeida, J.C.H.; Tupinambá, M.; Siga, O., Jr.; Trouw, R.A.J. Correlation of Neoproterozoic terranes between the Ribeira Belt, SE Brazil and its African counterpart: Comparative tectonic evolution and open questions. In *West Gondwana Pre-Cenozoic Correlations across the South Atlantic Region*; Pankhurst, R.J., Trouw, R.A.J., Brito-Neves, B.B., de Wit, M., Eds.; Geological Society of London: London, UK, 2008; Volume 294, pp. 211–232.
24. Kirsch, R. (Ed.) *Groundwater Geophysics: A Tool for Hydrogeology*; Springer: Berlin/Heidelberg, Germany, 2006.
25. Kuras, O.; Beamish, D.; Meldrum, P.I.; Ogilvy, R.D. Fundamentals of the capacitive resistivity technique. *Geophysics* **2006**, *71*, G135–G152. [[CrossRef](#)]
26. Cavenaghi, V.L.S. Caracterização Geométrica de Alvos Rasos no Sítio Controlado de Geofísica Rasa-II-IAG/USP Através do Uso de Resistividade Capacitiva. Master's Thesis, Universidade de São Paulo, São Paulo, Brazil, 2017; 148p. [[CrossRef](#)]
27. Carmona, E.; Barbosa, A.; Ustra, A.; Elis, V.; Mendonça, C. Aplicação do método resistivo-capacitivo para investigação de uma área contaminada por creosoto. In Proceedings of the VIII Simpósio Brasileiro de Geofísica, Salinópolis, Brazil, 18–20 September 2018; Available online: https://sbgf.org.br/mysbgf/eventos/expanded_abstracts/VIII_SimBGf/Aplica%C3%A7%C3%A3o%20do%20m%C3%A9todo%20resistivo-capacitivo%20para%20investiga%C3%A7%C3%A3o%20de%20uma%20%C3%A1rea%20contaminada%20por%20creosoto.pdf (accessed on 14 December 2023).
28. Osella, A.; Bongiovanni, M.V.; De La Vega, M. Development of a Geoelectric Device of Capacitive Contact for Studying Archaeological Targets in Very Resistive Zones. In *Proceedings of the Near Surface Geoscience 2012—18th European Meeting of Environmental and Engineering Geophysics, Paris, France, 3–5 September 2012*; EAGE Publications BV: Utrecht, The Netherlands, 2012; p. cp-306. Available online: <https://www.earthdoc.org/content/papers/10.3997/2214-4609.20143455> (accessed on 14 December 2023).
29. McNeill, J.D. Principles and Application of Time Domain Electromagnetic Techniques for Resistivity Sounding. 1994. Available online: <http://www.geonics.com/pdfs/technicalnotes/tn27.pdf> (accessed on 14 December 2023).
30. Porsani, J.L. Ground Penetrating Radar (GPR): Proposta Metodológica de Emprego em Estudos Geológico-Geotécnicos Nas Regiões de Rio Claro e Descalvado–SP. Ph.D. Thesis, São Paulo State University, São Paulo, Brazil, 1999; 145p.
31. Annan, A.P. *Ground Penetrating Radar Workshop Notes*; Sensors & Software Inc.: Mississauga, ON, Canada, 2001.
32. Porsani, J.L.; Oliveira, N.C.; Penna, N.S.; Costa, V.H.H.; Stangari, M.C.; Sousa, C.C.B.F. Emprego do GPR para orientar a exploração de mármore na região de Campos do Jordão, SP: Resultados preliminares. In *Anais do SimSBGf; IX Simpósio Brasileiro de Geofísica*; SBGf: Curitiba, Brasil, 2022; Available online: <https://www.sbgf.org.br/simposio/progfinal.pdf> (accessed on 14 December 2023).
33. DEMIN. Projetos e Linhas de Pesquisa. Departamento de Engenharia de Minas, UFMG. 2023. Available online: <https://www.demin.ufmg.br/textoproj01.php> (accessed on 20 January 2023).
34. Pereira, T.F. Proposta de Retomada e Expansão para uma mina de Calcário. Unipampa, Tecnologia em Informação. 2017. Available online: <https://cursos.unipampa.edu.br/cursos/tecnologiaemmineracao/files/2019/08/proposta-de-retomada-e-expansao-para-uma-mina-de-calcario.pdf> (accessed on 20 January 2023).
35. Curi, A. *Minas a Céu Aberto: Planejamento de Lavra*; Oficina de Textos: São Paulo, Brazil, 2014.
36. Leite, T.M.G. Comparação Entre Métodos de Cálculo de Cava Final: Lerchs Grossmann vs. Sequenciamento Direto de Blocos. Monografia, Centro Federal de Educação Tecnológica de Minas Gerais. 2017. Available online: https://www.eng-minas.araxa.cefetmg.br/wp-content/uploads/sites/170/2018/05/Tiago_Mozart_FINAL1.pdf (accessed on 8 June 2023).
37. Martins, A.C.C. Impacto da Aplicação da Geofísica no Planejamento de Lavra da Mineração de Pequena Escala. Ph.D. Thesis, Universidade de São Paulo, São Paulo, Brazil, 2017; 107p. [[CrossRef](#)]
38. Micromine. Micromine Beyond: Pit Optimisation. 2023. Available online: <https://www.micromine.com/micromine-training-pit-optimisation/> (accessed on 24 April 2023).
39. Porsani, J.L.; Sauck, W.A.; Souza, A.O., Jr. GPR for mapping fractures and as a guide for the extraction of ornamental granite from a quarry: A case study from southern Brazil. *J. Appl. Geophys.* **2006**, *58*, 177–187. [[CrossRef](#)]

Disclaimer/Publisher's Note: The statements, opinions and data contained in all publications are solely those of the individual author(s) and contributor(s) and not of MDPI and/or the editor(s). MDPI and/or the editor(s) disclaim responsibility for any injury to people or property resulting from any ideas, methods, instructions or products referred to in the content.